



Grant Agreement Number 243964

QWeCI:

Quantifying Weather and Climate Impacts on Health in Developing Countries

D1.2b: Assessment of ECMWF interim reanalysis products for target countries

Start date of project: 1st February 2010

Duration: 42 months

Lead contractor: ECMWF

Coordinator of deliverable: F. Di Giuseppe (ECMWF)

Authors: F. Di Giuseppe (ECMWF) AM
Tompkins (ICTP)F Molteni
(ECMWF)

Evaluation of deliverable:

Due date M24

Date of first draft M23

Start of review M24

Deliverable accepted: M24

Project co-funded by the European Commission within the Seventh Framework Programme (2007-2013)		
Dissemination Level		
PU	Public	PU
PP	Restricted to other programme participants (including the Commission Services)	
RE	Restricted to a group specified by the consortium (including the Commission Services)	
CO	Confidential, only for members of the consortium (including the Commission Services)	

Contents

1	Introduction	8
2	Weather systems over Africa	10
3	Verification set-up	13
3.1	Data	13
3.2	Model configurations	14
3.3	Validation period	15
4	Seasonal forecast verification	16
4.1	Precipitation	16
4.2	Surface temperature	27
5	ERA-I verification	33
6	Conclusion	35

List of Figures

2.1	African climatic zones relevant in terms of large scale precipitation and temperature. The countries part of the QWeCI demonstration project are highlighted in different colours; namely Senegal (red), Ghana (green), Malawi (Yellow)	11
4.1	SYS3 10 ensemble mean precipitation bias relative to GPCP v2 for JJA from 2000 to 2009. The hashed area indicate regions where the difference is significant at the 95% level, and negative contours are shown with dashed lines.	17
4.2	Same as figure 4.1 but for the CMPA dataset from Xie and Arkin (1997).	18
4.3	Same as figure 4.1 but for DJF.	19
4.4	Same as figure 4.3 but for the CMPA dataset from Xie and Arkin (1997)	20
4.5	SYS4 10 ensemble mean precipitation bias relative to GPCP v2 for JJA from 2000 to 2009. The hashed area indicate regions where the difference is significant at the 95% level, and negative contours are shown with dashed lines.	21
4.6	Same as figure 4.5 but for DJF.	22
4.7	Top of atmosphere (TOA) infrared flux biases between SYS-4 and CERES measurements. Left panel: mean JJA period. right panel: mean DJF period.	23
4.8	Left panel: TOA SW radiative flux bias and in the right panel: Total cloud cover bias in absolute %. The plot refers to SYS-3 and the year 2006 is taken as an example.	24
4.9	Left panel: TOA SW radiative flux bias and in the right panel: Total cloud cover bias in absolute %. The plot refers to SYS-4 and the year 2006 is taken as an example.	25
4.10	Left panel: SYS-3 total column liquid water path biasfor the JJA 2006 period. Right panel: SYS-4 total column liquid water path bias for the JJA 2006 period	26
4.11	Left panel: SYS-3 bias for the 10m wind compared to Quikscat measurements. Right panel: same but for SYS-4. The period refers to JJA 2006.	27
4.12	System 4 surface temperature bias relative to ERA-I reanalysis for JJA from 2000 to 2009. The hashed area indicate regions where the difference is significant at the 95% level, and negative contours are shown with dashed lines.	28
4.13	Same as figure 4.12 but for the DJF period	29
4.14	Reliability diagrams over Africa (only land points) for SYS-4 initialised the 1st of August 2011 and for months 2 to 4 lead times. Left plot lower tercile. Right plot: upper tercile	30
4.15	ERA-I mean precipitation bias relative to GPCP v2 for JJA from 2000 to 2009. The hashed area indicate regions where the difference is significant at the 95% level, and negative contours are shown with dashed lines.	31
4.16	ERA-I mean precipitation bias relative to GPCP v2 for JJA from 2000 to 2009. The hashed area indicate regions where the difference is significant at the 95% level, and negative contours are shown with dashed lines.	32
5.1	Mean ERA-I fields from the last ten year period 1999-2008 compared to the first ten year mean 1989-1998.	33

5.2	Comparison between ERA-I, the operation Ensemble Forecast system (EPS) and GPCP dataset. The upper panel shows the differences between ERA-I and the GPCP climatology for June while the lower panel show the correlation anomaly between the three datasets	34
5.3	Same as figure 5.2 but for July.	34

List of Tables

3.1	Datasets used for validation	14
3.2	Key differences between the operational SYS-3 and SYS4	14

In this report the key systematic errors of the ECMWF model over Africa are described by comparing the new operational seasonal forecasting system (SYS-4) with the previous system 3 (SYS-3) which used the same model cycle of the ECMWF re-analysis product ERA-Interim (ERA-I). Focal points of this analysis are (1) documenting the climate errors and forecast skill of the latest seasonal system, (2) the evolution of model errors across the two systems, (3) characteristics of the growth of errors throughout the forecast including monthly, and seasonal time scales.

Results are presented for temperature and humidity fields, cloud related parameters and the atmospheric circulation. Furthermore, misrepresentation of some key phenomena related to the monsoon activities in the west Africa and the south-east Africa regions are discussed. SYS-3 seasonal forecast system suffered from a systematic bias whereby monsoon rains were constantly shifted to the south. This is thought to be related to the cause of a dry bias in the precipitation amount predicted by short range forecasts initialised from analysis over the Sahel. The magnitude of these model errors has been reduced considerably in the new system. The spatial structure of systematic model errors, however, remains more or less unchanged for most of the parameters.

1 Introduction

The QWeCI project aims, through the identification of relationships between atmospheric variables and the occurrence of vector borne diseases (malaria and the Rift Valley Fever) to develop a prediction system tailored for disease prevention. This report follows the D1.2a QWeCI report, evaluating the skill of ECMWF Integrated Forecasting System (IFS) seasonal forecast and reanalysis systems in predicting weather evolution at different lead times over Africa. IFS has been in fact selected as the driving forecasting system to provide the atmospheric fields (mainly precipitation and temperature) to force the malaria models which will be used into QWeCI. In this report we only address the direct use of global circulation model outputs, whereas the possibility to correct this model outputs using observed climatological means will be included in future reports.

The ECMWF forecast system currently consists of three operational components, namely a 10 day deterministic forecast, a 15 day variational ensemble prediction system (VarEPS) forecast that is extended to 32 days once each week (Vitart *et al.*, 2008, commonly referred to as the VarEPS-monthly forecast system)¹, and an ensemble seasonal forecast system that once a month issues a 7 month (extended to 13 months four time a year) prediction.

In this report we focus on the monthly to seasonal lead time scale. Therefore only products from the VarEPS-monthly and the seasonal forecasting system will be analysed. The reason being that the forecast at shorter lead times would provide information at lead times too short to permit actions to be taken by the health prevention sector. The lead time requirement was specified by the QWeCI project partners at the onset. There is a substantial difference between the two systems which needs to be highlighted. The atmospheric model component of the VarEPS-monthly usually updated several times per year, each identified with a code XXRY, where Y is the release (R) of each code cycle XX. Some of these atmospheric model upgrades are not relevant for the seasonal forecasting system; monitoring or incorporating new observations into the analysis system, implementing new analysis system improvements or operational technical changes. Nevertheless, a number of these upgrades incorporate major changes to the model physics parameterisations which are mostly evaluated and developed in the uncoupled atmosphere-only framework.

Due to the frequent updates that are made to the model physics and data assimilation system, each VarEPS-monthly forecast ensemble integration also runs a 5-member hindcast suite of integrations for the same months over the previous 18 years for calibration purposes. Thus, for every month a set of 19 years are available using an identical system. The seasonal forecast system also has an extensive hindcast suite (50 members in SYS4) but the lower resolution and the less recent model cycle (the seasonal system atmospheric model is updated less frequently, every 3 to 5 years) implies that the skill is lower relative to the monthly system in the overlapping first four weeks. Moreover the much more frequent updates to the monthly system compared to the seasonal system imply that the bias characteristics of the two diverge over time, only reconverging when the seasonal system is revised.

¹from October 2011 the extended monthly integrations have been conducted twice a week.

In parallel to producing operational forecast, ECMWF is also conducting extensive reanalysis projects. While the analysis are used primarily to initialise the operational forecasts they are also a valuable tool for subsequent meteorological and climatological studies provided that inconsistency due to model changes and observation systems upgrades are removed. A reanalysis project therefore involves reprocessing observational data spanning an extended historical period. It makes use of a consistent modern analysis system, to produce a dataset that to a certain extent can be regarded as a "proxy" for observation with the advantage of providing coverage and time resolution often unobtainable with normal observational network. The latest global atmospheric reanalysis produced by ECMWF which extends from 1 January 1979 to the present date Dee *et al.* (2011) is ERA interim (ERA-I). This dataset will be analysed here in its capability to represent the Africa climate, its seasonal and intra-seasonal variability. The ERA-I configuration has a spectral T255 horizontal resolution (about 80 km in the grid-point space) with 60 model levels.

The report mostly concentrates on precipitation and temperature and provides in the following chapters: i) a review of ECMWF forecasting system and of available datasets for model validation; ii) skill of the new seasonal forecast (SYS-4) and for comparison the old one (SYS-3) in predicting Africa weather conditions, and iii) skill of ERA-I re-analysis to be used as an observational proxy for temperature and precipitation over Africa.

2 Weather systems over Africa

The atmospheric circulation over the Africa continent is to be considered in spatial continuity with conditions over the adjacent Eastern Atlantic. Most of the precipitation over this continent is then controlled by the south to north and back displacement of the Inter Tropical Convergency Zone (ITCZ), the intensity of the low level Tropical Easterly jet and the flow disturbances in the high level African Easterly jet. The interaction of all these large scale features combined with local produced convection generates three climatic zones relevant in terms of large scale precipitation and temperature; the well pronounced West Africa monsoon system, the less intense East Africa monsoon and the central Africa seasonal variation (see figure 2.1 for the location of these areas).

The rainfall field over **West Africa** is characterised by a zone of maximum precipitation that migrates north and south throughout the course of the year. This zone lies to the south of the the ITCZ and its seasonal excursion roughly parallels the seasonal excursion of the ITCZ. The rain-belt is the loci of disturbances that are dynamically linked to the mid-level African Easterly Jet (AEJ). Westward propagating mesoscale disturbances, termed cloud clusters, are the dominant convective system. Certain environmental factors, such as vertical wind shear, buoyant energy, low-level jets, and latitude, determine whether convection organises into these long-lived systems (Laing and Fritsch, 1993). The frequency of cloud clusters and the amount of rainfall associated with them is modulated by transient synoptic-scale African or easterly waves (Houze Jr and Betts, 1981). These waves originate as a consequence of a joint baroclinic-barotropic instability associated with the vertical and horizontal shear of the midtropospheric AEJ. The waves, as well as the cloud clusters, are generally confined to a relatively narrow latitudinal zone south of the jet (Laing and Fritsch, 1993; Albignat and Reed, 1980; Burpee, 1972). This zone corresponds to the region between the axes of the AEJ and the higher level Tropical Easterly Jet. Their growth and development is influenced by several factors, including the magnitude of the horizontal and vertical shear of the AEJ (Rennick, 1981), and latent heat release (Norquist *et al.*, 1977). Although the shear instability associated with the jet is present throughout the rainy season, the waves appear to contribute to the development of large-scale rainfall systems only during late boreal summer. For the waves to organize rainfall, they must produce moisture convergence and be reasonably close vertically to the moist layer. Past studies have suggested that in the Sahel, these prerequisites are present only in late summer. This fact may help to explain the contrast between the rainfall regimes in June-July and August-September, noted in several studies, and the fact that mesoscale convective complexes are much more frequent during the latter period. Areas somewhat south-east of West Africa (Central Africa Republic, Chad, and Sudan) and west (Nigeria and other countries of the Guinea Coast) are meteorologically controlled by the same processes and features that influence Sahelian West Africa and peak rainfall occurs in the boreal summer, when the ITCZ moves to its far northern limits.

Central Africa extending westward to Cameroon and eastward to the Rift Valley highlands, in contrast, experiences a strongly bimodal annual cycle, coincident with both the northward and southward passage of the ITCZ. Peak rainfall tends to be in the two transition seasons. This zone may have many common features with eastern equatorial Africa, generally termed **East Africa** where a small monsoon cycle is present with peak precipitation occurring during boreal winter. Rainfall variability in these regions shows

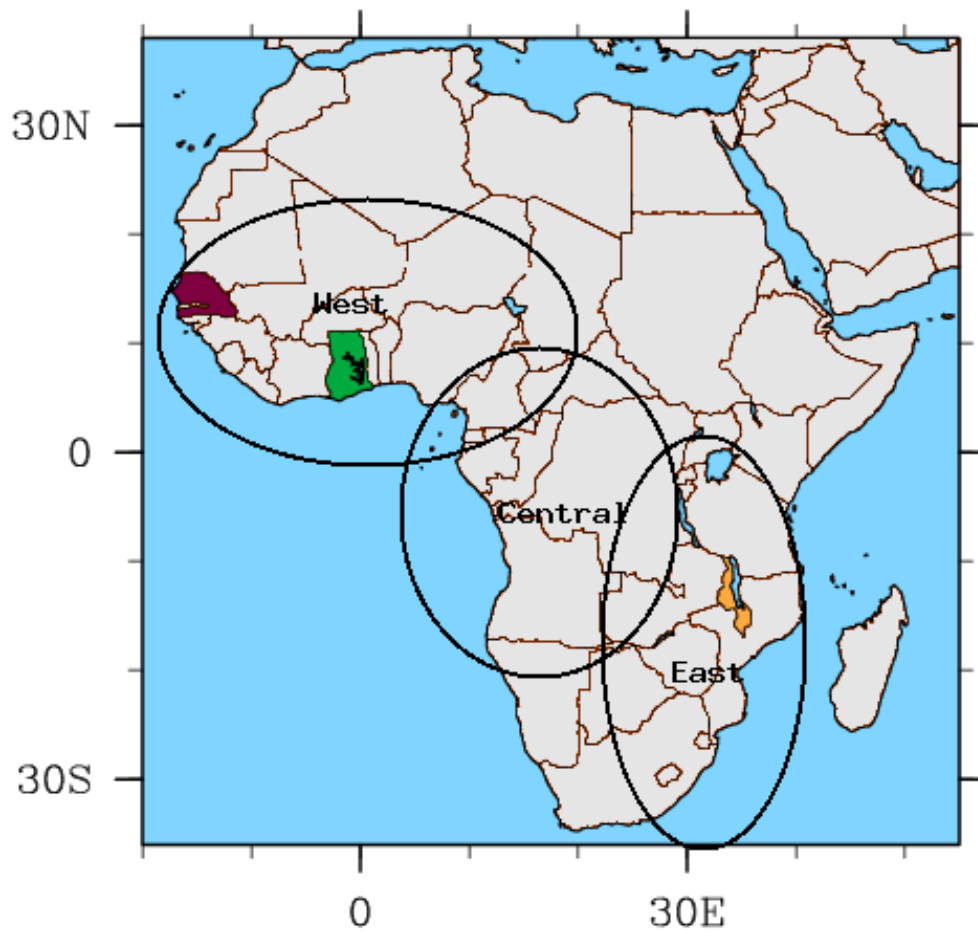


Figure 2.1: African climatic zones relevant in terms of large scale precipitation and temperature. The countries part of the QWeCI demonstration project are highlighted in different colours; namely Senegal (red), Ghana (green), Malawi (Yellow)

some commonalities with that over East Africa. The variance spectra for rainfall throughout the region show very strong peaks on the order of 5-6 yr and generally smaller peaks at roughly 3.5 and 2.3 yr, the same peaks found in the Southern Oscillation. The variability is generally out of phase with that in the Sahel [i.e., dry (wet Sahel corresponds to wet (dry) Central Africa]. Although wave activity has not been identified, rainfall tends to be organized into mesoscale convective systems (MCSs) analogous to those in Sahelian West Africa. Very little is still known about the modulation introduced by the Rift Valley highlands on the large scale flow

3 Verification set-up

3.1 Data

The dataset used for validation purposes is summarised in table 3.1. As the report mostly concentrates on precipitation forecast biases, three different datasets are used for this parameter. The Global Precipitation Climatology Project (GPCP) merges station data with Satellite information and thus suffers less from sampling bias in regions with sporadic data availability. The TRMM rainfall retrieval modules is a "combined algorithm", meaning that it combines inputs from the 2 instruments whose measurements are directly responsive to the rain characteristics: the 13.8 GHz Precipitation Radar (PR), and the 9-channel passive TRMM Microwave Imager (TMI). The "instantaneous" combined algorithm estimates the 3-dimensional structure of the particle size distribution within the PR swath, based on the PR and TMI measurements within the swath. The "daily area-averaged" combined algorithm, daily averages on a 0.5-degree grid. These Special Sensor Microwave/Imager (SSM/I) are produced as part of NASA's Pathfinder Program. Remote Sensing Systems generates SSM/I data products using a unified, physically based algorithm to simultaneously retrieve *ocean* wind speed (at 10 meters), water vapour, cloud water, and rain rate. Finally the Climate Prediction Centre (CPC) Merged Analysis of Precipitation product for precipitation is used (CMAP, Xie and Arkin (1997)). All radiation measurements are provided by the Clouds and Earth's Radiant Energy System (CERES) mission. CERES products include both solar-reflected and Earth-emitted radiation from the top of the atmosphere to the Earth's surface. Cloud properties are determined using simultaneous measurements by other instruments such as the Moderate Resolution Imaging Spectroradiometer (MODIS) and the Visible and Infrared Sounder (VIRS).

All daily data are used and even if they have greater uncertainties, but they are used to provide information concerning the sub-seasonal temporal variations. For statistical significance estimates when comparing model mean fields, very simple fixed error estimates are used of 0.05 for ISCCP total cloud cover (Rossow *et al.*, 1993) and 15% of rainfall for GPCP v2 (Adler *et al.*, 2003). For monthly mean fields the uncertainty of scatterometer winds is estimated as 0.7 m s^{-1} (Hans Hersbach, ECMWF, personal communication). Error estimates for CERES monthly radiative budgets at the top of the atmosphere were given as 2.5 W m^{-1} for shortwave and 1.9 W m^{-1} for longwave by Wielicki *et al.* (1995).

For a number of fields, surface rainfall for example, several validation products are available and used. This gives an indication at least of the zero-order uncertainty in the observations. The plots shown provide an indication of mean bias and rms errors between the model and observations. In all cases no attempt is made to apply any bias correction to the observational product. Note that while a subset of these products could not be used as an independent metric of the forecast model over short forecast ranges since they are actively assimilated in 4D-VAR, they can be safely used in these tests where the model has achieved a quasi-equilibrium state and has effectively forgotten the initial conditions.

Table 3.1: Datasets used for validation

Parameter	Data	Resolution	References
SST	OISST	1.0°	Reynolds <i>et al.</i> (2002)
Cloud Cover	ISCCP	2.5°	Rossow and Schiffer (1991)
Radiative Flux	CERES	2.5°	Wielicki <i>et al.</i> (1996)
10m Winds	Quikscat	25 km	Hoffman and Leidner (2005)
10m Winds	SSM/I	1.0°	Wentz (1997)
Precipitation	TRMM	0.5°	Mitchell and Jones (2005)
Precipitation	GPCP	2.5°	Huffman <i>et al.</i> (1995)
Precipitation	SSM/I	0.1°	Wentz (1997)
Precipitation	CMPA	0.1°	Xie and Arkin (1997)

Table 3.2: Key differences between the operational SYS-3 and SYS4

	System 3	System 4
Ocean model	HOPE	NEMO
IFS cycle	31r1	36r4
IFS horizontal resolution	TL159	TL255
IFS vertical resolution (TOA)	L62 (0.5 hPa)	L91 (0.01 hPa)
IFS model unc stoch schemes	1-lev SPPT	3-lev SPPT and SPBS
Fc mem run monthly for 7m	41	51
Fc mem ext to 13m (FMAN)	5	15
Hindcast years	25 (1981-2005)	30 (1981-2010)
Hindcast members	11 (7m) / 5 (7-13m)	15 (0-13m)

3.2 Model configurations

The atmospheric model of the old SYS-3 is based on version number 31R1. This cycle was operational in the medium range and ensemble systems during 2006, and was also used for the interim reanalysis. The resolution is T_L159 (120 km) with 62 vertical sigma levels. The atmosphere is coupled to the Hamburg Ocean Primitive Equation (HOPE) ocean model running with 29 vertical levels (Wolff *et al.*, 1997).

The new seasonal forecasting system at ECMWF (SYS-4) came to life in August 2010 with the release of the hindcast set. Operational forecast is issued since 1st November 2011. System 4 is based on a more recent atmospheric model version (IFS model cycle 36r4), higher resolution forecasts with a higher top of the atmosphere, more members, and a larger hindcast data set (see Table below). System 4 initial perturbations are defined (as in System 3) with a combination of atmospheric singular vectors and an ensemble of ocean analyses. Atmosphere model uncertainties are simulated using the 3-time level stochastically perturbed parameterised tendency (SPPT) scheme and the stochastic back-scatter scheme (SPBS) operational in the EPS (System 3 used only a 1-time version of SPPT). System 4 uses NEMO instead of HOPE as its ocean component (with the same resolution), with initial conditions generated by the Near Real Time (NRT) NEMOVAR suite instead of HOPE/OI. In February, May, August and November, 15 of the 51 members are extended to 13 months. Key differences between the operational SYS-3 and SYS4 are given in table 3.2

The atmospheric model used for ERA-I is the same as the one employed for SYS-3 and is based on version number 31R1. This cycle was operational in the medium range and ensemble systems during 2006. The resolution is T_L255 (80 km) with 91 vertical sigma levels. ERA-I as initially described is an 'interim' reanalysis of the period 1979-present in preparation for the next-generation extended reanalysis to replace ERA-40 (Dee *et al.* (2011)). The ERA-I archive is more extensive than that for ERA-40, e.g. the number of pressure levels is increased from ERA-40's 23 to 37 levels and additional cloud parameters are included. There are several differences in data assimilation and use of observations between ERA-40 and ERA-I. The main advances in the ERA-I data assimilation compared to ERA-40 are the 12 hour 4D-Var T255 horizontal resolution, the better formulation of background error constraint, the new humidity analysis, improved model physics, data quality control that draws on experience from ERA-40 and JRA-25, variational bias correction of satellite radiance data, and other improvements in bias handling, more extensive use of radiances, and improved fast radiative transfer model.

While ERA-I uses mostly the sets of observations acquired for ERA-40, some supplementary data has been introduced for later years from ECMWF's operational archive. Namely the new ERS altimeter wave-height dataset that has been acquired from ESA, providing data of more uniform quality than the Fast Delivery Dataset used from August 1991 onwards in ERA-40 Winds and clear-sky radiances. Moreover EUMETSAT provided reprocessed winds and clear-sky radiances from Meteosat-2 (1982-1988) for ERA-40 and has reprocessed later Meteosat data for ERA-I Ozone profiles. Also reprocessed GOME data from the Rutherford Appleton Laboratory will provide ozone profile information from 1995 onwards and radio occultation measurements are included from CHAMP, GRACE and COSMIC since 2006.

3.3 Validation period

As described in section 2 the main interest is the West African monsoon period which occurs during the boreal summer July to August (JJA), and the East African monsoon which occurs during the boreal winter. The analysis is mostly restricted to the JJA and the DJF period. To be able to understand the performances of the model in different large scale flow conditions 8 to 10 years from 2000 to 2010 of data (depending on the availability of data in the different dataset) are analysed.

For the seasonal forecast this implies to be restricted to the 1st May forecasts, implying a 2-4 month lead time for the West Africa monsoon and starting date the 1st of November for the East Africa monsoon. This start date is also pertinent, since it is the 1st May integrations that contribute to the PRESAO consensus forecast process. Each forecast consists of 10 ensemble member integrations. The ensemble members are initialised with perturbed SSTs created by introducing surface wind anomalies in the ocean analysis system that represent the wind uncertainty. Vialard *et al.* (2005) compared this perturbation method to other alternatives and noted that all methods led to a lack of spread in the 2-4 month range, pointing to multi-model ensembles as the solution.

For ERA-I the JJA and DJF monthly means are extracted using the precipitation taken from the first 24hr forecasts starting at 00UTC daily. This is the forecast window closest to the initial conditions provided by the data assimilation system; however these should be considered as short-range forecasts and not analysis.

Please note that during the 10 years under examination there were two weak El Niño episodes in 2004 and 2006 and one weak La Niña episode in 2007.

4 Seasonal forecast verification

4.1 Precipitation

Figures 4.1 to 4.4 show the average seasonal precipitation for JJA and DJF from 2000 to 2009 in system 3. The mean precipitation is compared with both GPCP and the CMAP datasets (CMAP dataset extends to 2010). It reveals that the model is able to reproduce the distribution of rainfall reasonably well for both periods with the peak over the West African coast in addition to the orographically forced local maxima over the Cameroonian and Ethiopian highlands during JJA. There are obvious shortcomings in the monsoon precipitation climatology, with an underestimation over Eastern Africa (although station data is sparse in some regions there, especially for recent periods). It is apparent that the rain in the West African monsoon is displaced too far south in the model. It is also evident that in areas where in situ observations are few large discrepancies can be presents between datasets. The use of GPCP data would, for example, highlight a larger bias. Similar features are still presents in the new system 4 as shown by figures 4.5 and 4.6 where the JJA and DJF precipitations compared to GPCP dataset are reported.

The top of atmosphere (TOA) infrared flux is often used as a proxy for convective activity. The difference map (Fig. 4.7) for SYS4 shows a large region over West Africa where the biases are negative (TOA IR flux is assigned positive downward), signifying too high outgoing long-wave radiation. This agrees with the previous precipitation biases, indicating a lack of deep convection in the Sahel in this model cycle, although it should be recalled that TOA infrared flux information is used in the GPCP rainfall retrieval algorithms. The model biases in IR could also result from a lack of upper level cloud cover, not enough cloud ice, or deep convective clouds detraining at an altitude that is too low.

Past examination of model simulated Meteosat 11 micron channel brightness temperatures animations using the methodology of Morcrette (1989); Chevallier and Kelly (2002) indicates part of the error is due to the lack of high cirrus cloud that is advected northwards, cloud that would not produce surface precipitation. This raises the possibility that GPCP rainfall products, that use IR information in their retrievals, may in fact overestimate rainfall in the northern reaches of the Sahel affected by the advected cirrus cloud. Indeed, referring back to Figs 4.1 to 4.4, it is seen that GPCP rainfall amounts exceed the CMAP station data northward of 10N in each month from June to September.

Convection responds to a host of interacting dynamic and thermodynamic forcing which can impact the vertical thermodynamic profile and the associated convective available potential energy (CAPE) and convective inhibition (Parker, 2002). Thus the convective suppression may occur via atmospheric stabilisation by radiative heating or importation of dry air into the Sahel at low levels, such as would be the case if the heat low were too deep in the model simulation. Tompkins *et al.* (2005) found that an earlier atmospheric model version suffered from the convection migrating too far north during the forecast. Changes to the specified aerosol climatology in the region that reduced the aerosol optical depth over the Sahara and the Sahel had a strong impact on convection activity primarily through the short-wave (SW) radiation budget. The influence was two-fold, with a reduction in atmospheric SW heating

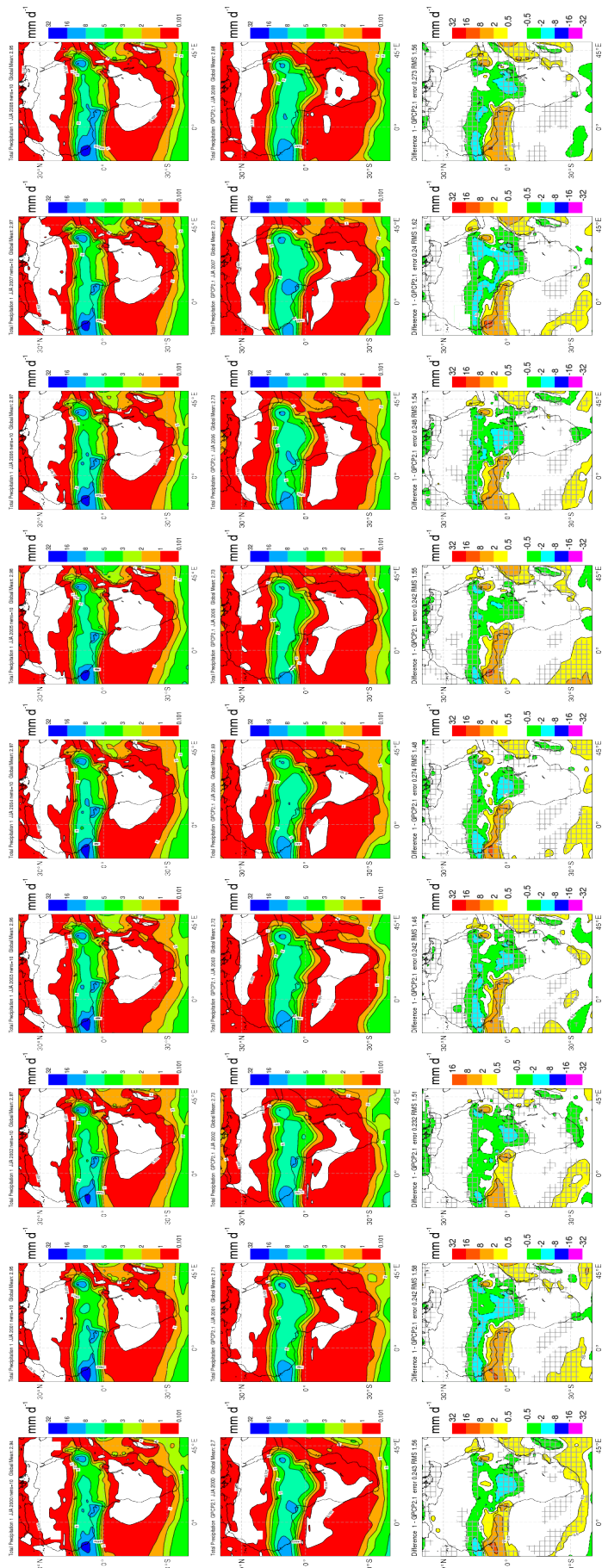


Figure 4.1: SYS3 10 ensemble mean precipitation bias relative to GPCP v2 for JJA from 2000 to 2009. The hashed area indicate regions where the difference is significant at the 95% level, and negative contours are shown with dashed lines.

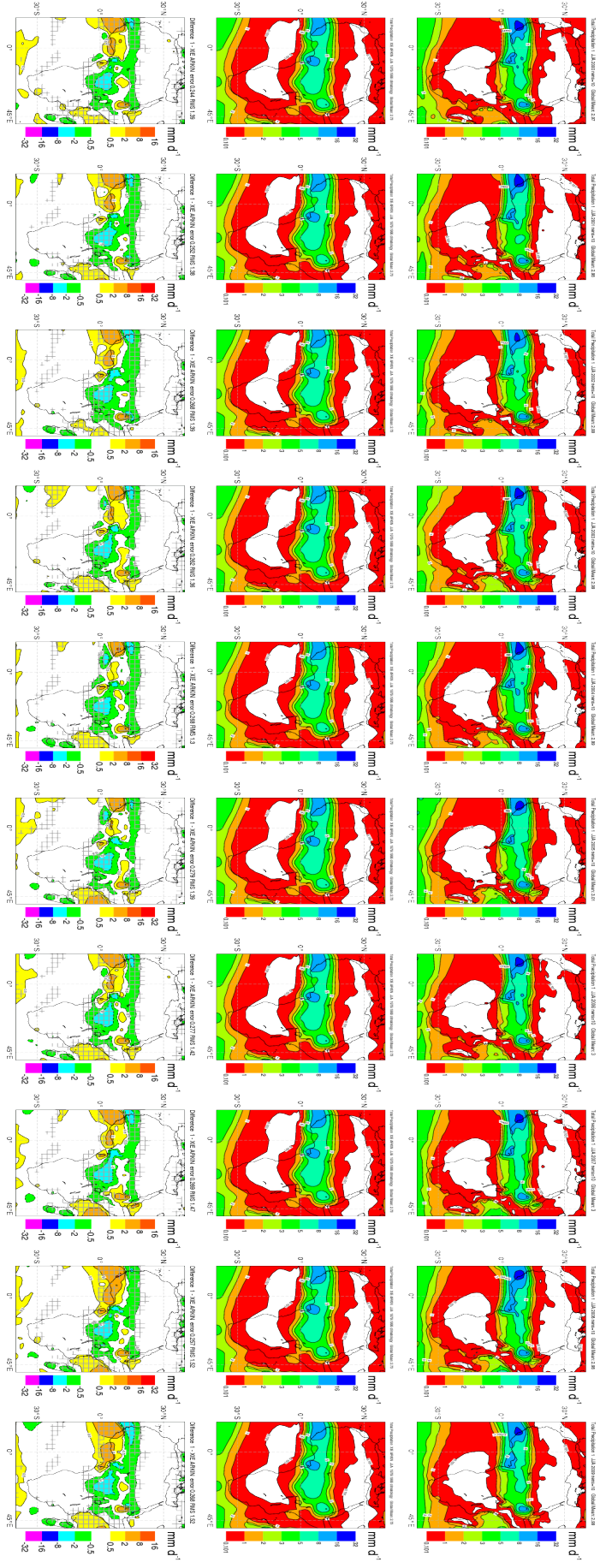


Figure 4.2: Same as figure 4.1 but for the CMA dataset from Xie and Arkin (1997).

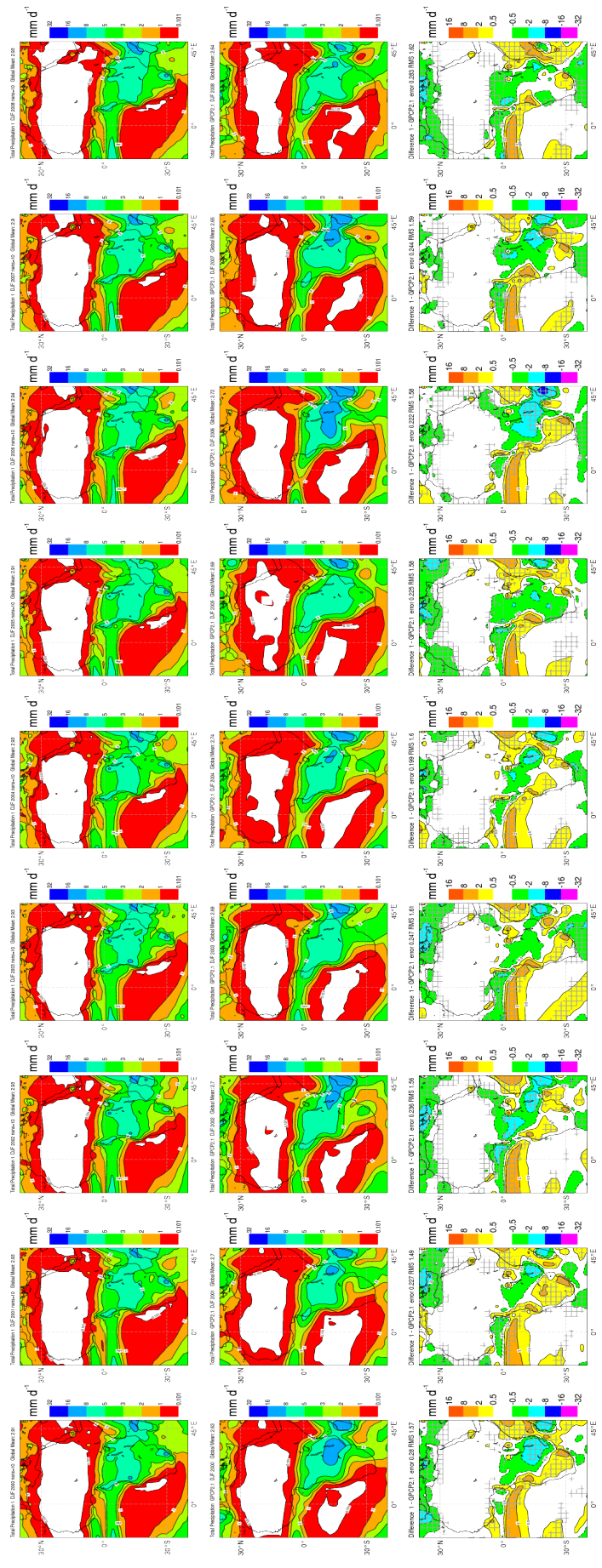


Figure 4.3: Same as figure 4.1 but for DJF.

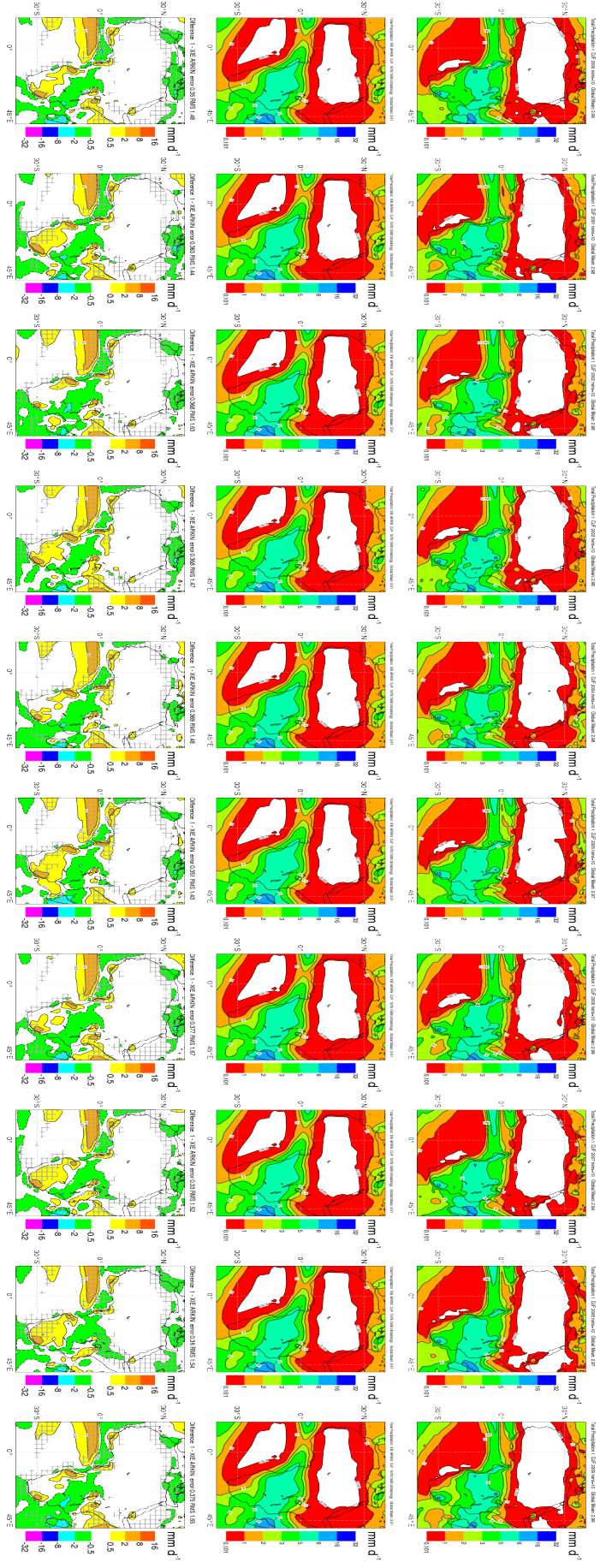


Figure 4.4: Same as figure 4.3 but for the CMA dataset from Xie and Arkin (1997)

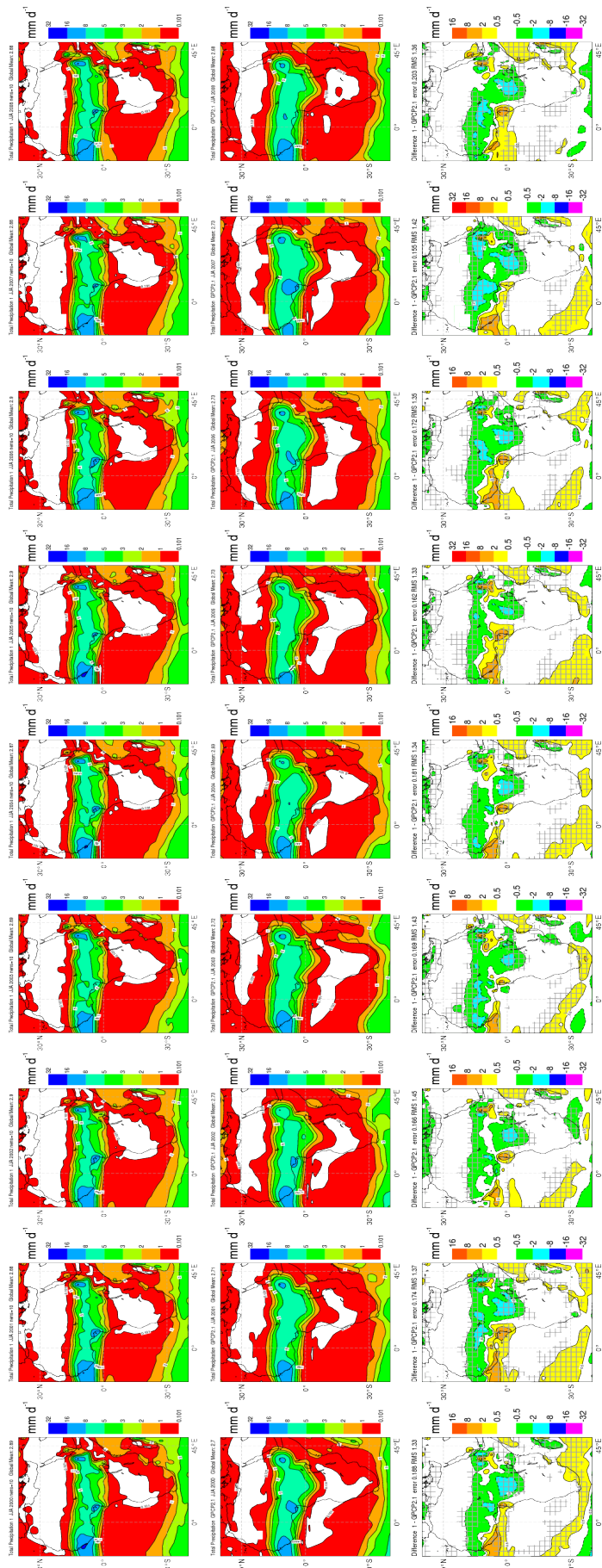


Figure 4.5: SYS4 10 ensemble mean precipitation bias relative to GPCP v2 for JJA from 2000 to 2009. The hashed area indicate regions where the difference is significant at the 95% level, and negative contours are shown with dashed lines.

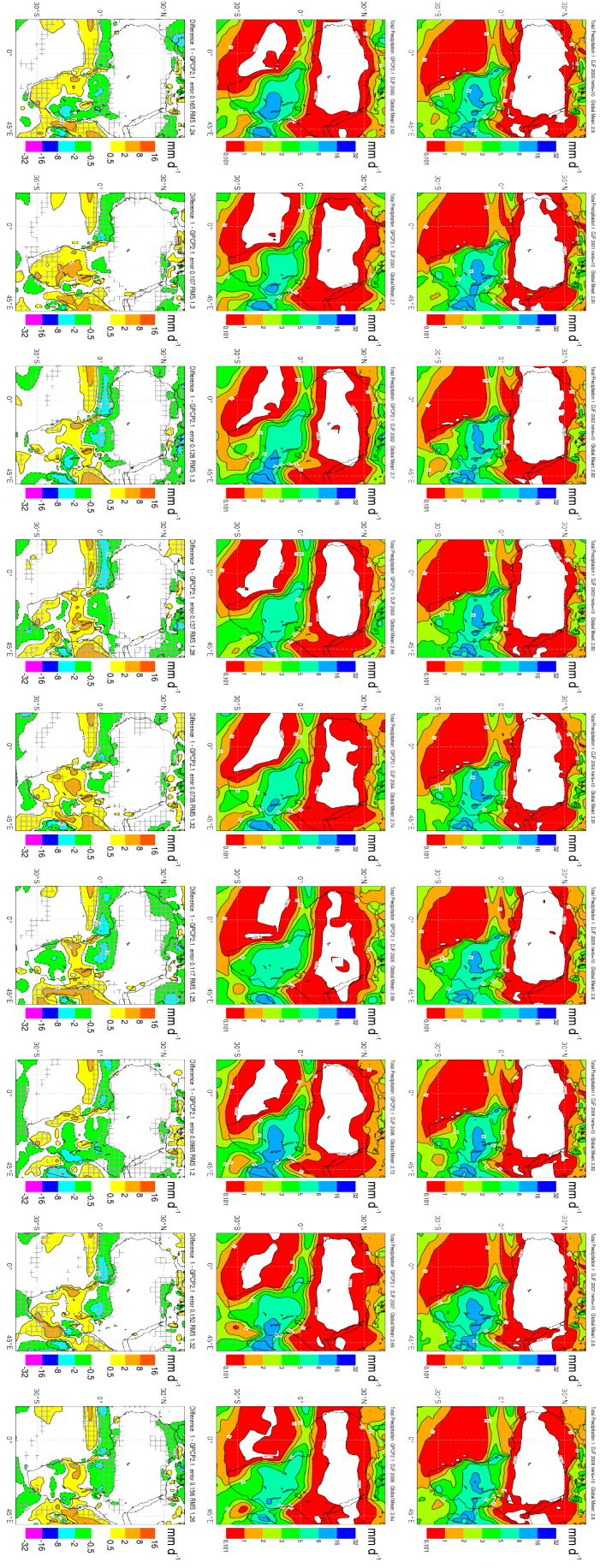


Figure 4.6: Same as figure 4.5 but for DJF.

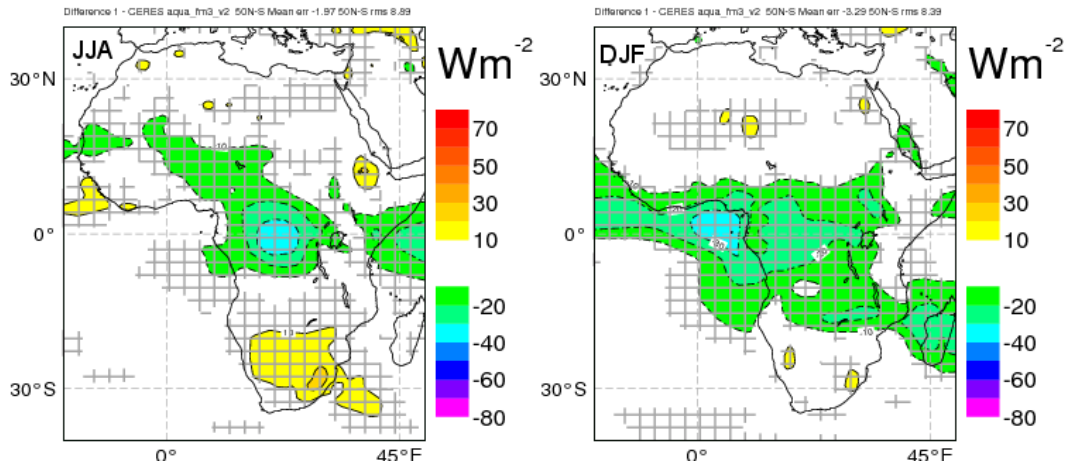


Figure 4.7: Top of atmosphere (TOA) infrared flux biases between SYS-4 and CERES measurements. Left panel: mean JJA period. right panel: mean DJF period.

through aerosol absorption leading to an increase in radiative stabilisation of the free troposphere. At the same time, the increase in the surface incoming solar radiation drives a deeper and more vigorous dry convective boundary layer over the heat low region. The reaction in the medium range forecast was the prevention of the northward propagation of deep convection and strengthened the forecasted African Easterly Jet.

Other reasons for the rainfall remaining too far south could be associated with factors that alter the low-level moist static energy budget, in which Thorncroft *et al.* (2003) documented biases in the model analyses using a older model cycle operational in the year 2000. A too-dry boundary layer could result from a dry land surface (shown to be potentially important in Douville and Chauvin, 2000), and replacing the land-surface scheme with a soil moisture history derived using observed precipitation has a small but nevertheless positive impact on rainfall in the Sahel, moving the rainband slightly northwards in the model simulations (Agusti-Panareda *et al.*, personal communication). The humidity and pressure gradients are also affected by the Saharan heat low thus representation of both land surface properties over the Sahara and dry convective processes are also likely to be important. A weakened monsoon flow, possibly by too much shear-driven mixing of the nocturnal jet (Parker *et al.*, 2005), may also play a role. To conclude, it is evident that deficiencies in the dry, shallow and deep convective schemes may be involved.

A further factor concerns the SSTs in the Gulf of Guinea. Warm SST anomalies in the Gulf of Guinea increase the boundary layer moist static energy of the low level monsoon flow, but primarily favour local deep convection over the Gulf, suppressing activity to the north. Warmer SSTs in the Gulf have been partly blamed for the extended decadal dry spell in the Sahel for example, along with a general warming in the Indian Ocean (Giannini *et al.*, 2003; Held *et al.*, 2005). On intra-seasonal timescales, the impact of the cold tongue development on enhancing the northward progression of the monsoon rain was shown in sensitivity tests by Okumura and Xie (2004), while the late development of the cold SSTs in the Gulf of Guinea were also suggested to play a role in the late onset of the monsoon in 2006 (Janicot *et al.*, 2008). By extension, models suffering from warm SST biases in the Gulf of Guinea will tend to exhibit increased convection over the Gulf and the Guinean coast at the expense of Sahelian rainfall. The mean seasonal forecast SST evolution over the monsoon period reveals the development of a strong positive bias over the tropical and southern Atlantic which exceeds 2K at its peak. The SST bias in the Northern

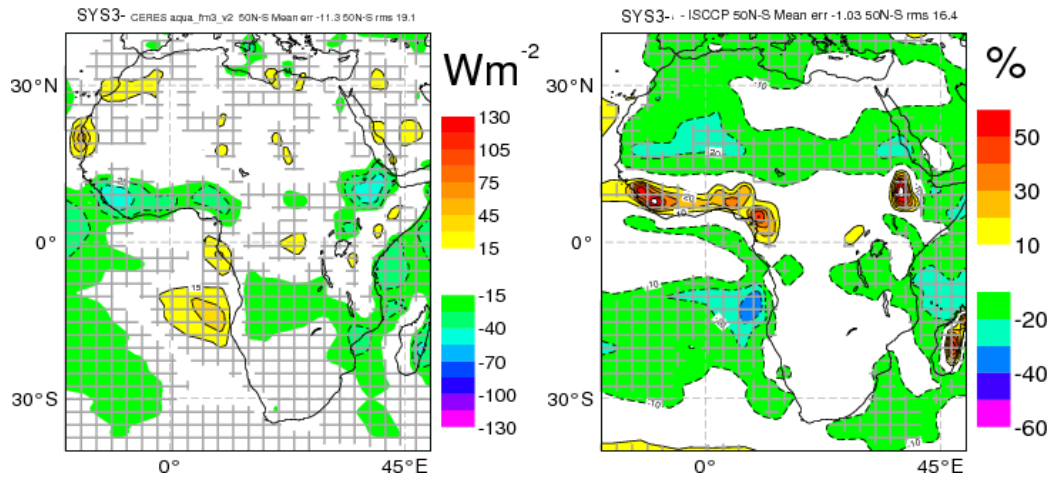


Figure 4.8: Left panel: TOA SW radiative flux bias and in the right panel: Total cloud cover bias in absolute %. The plot refers to SYS-3 and the year 2006 is taken as an example.

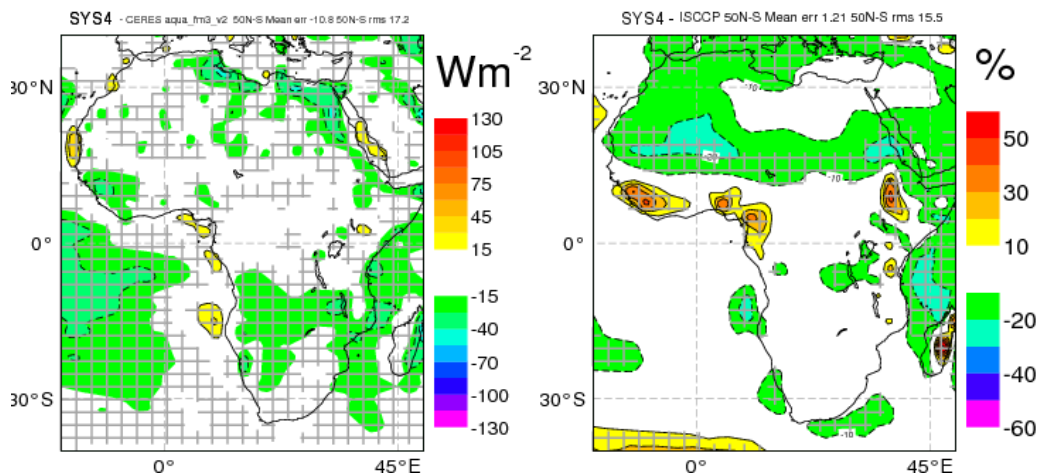


Figure 4.9: Left panel: TOA SW radiative flux bias and in the right panel: Total cloud cover bias in absolute %. The plot refers to SYS-4 and the year 2006 is taken as an example.

Atlantic ocean is negative on the other hand, which would also contribute to increase the north-south gradient of SST and further prevent northern migration of monsoon rainfall (Palmer, 1986). The SYS3 biases in the tropical Atlantic are seen to far exceed those anywhere in the Pacific basin, including the ElNino forecasting regions in the central and Eastern Pacific which form the benchmark for seasonal forecast system assessment.

The warm ocean bias coincides with the development of the cold tongue in the Eastern Atlantic (Mitchell and Wallace, 1992). The bias could be associated with the ocean model's representation of the mixed layer considering its 10m vertical resolution there, with Blanke and Delecluse (1993) highlighting the influence of the turbulent mixing formulation on SST in the region. The warm bias is not restricted to location of the cold tongue waters however, since there is also a significant warm bias in the northern hemisphere between the equator and the Guinea coastline at 5N.

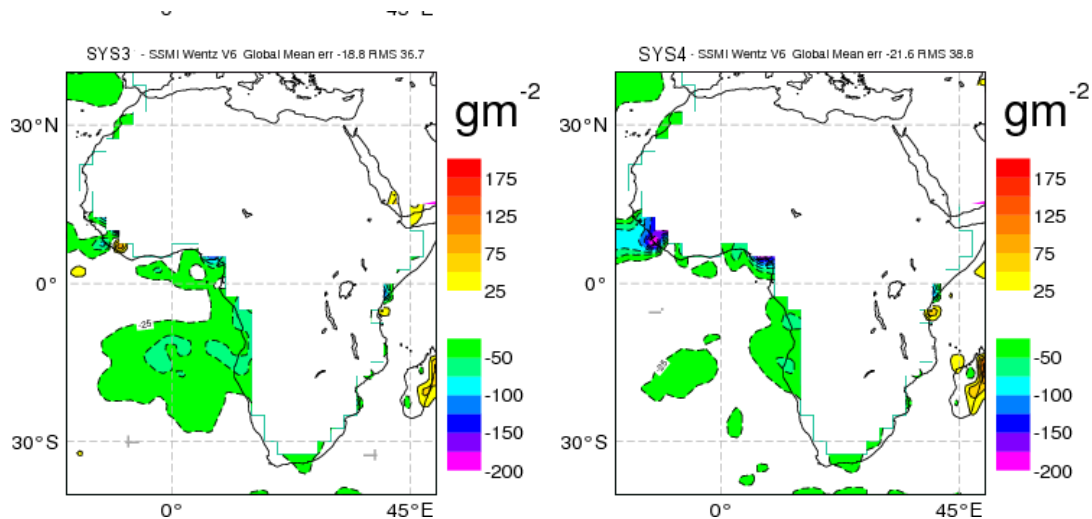


Figure 4.10: Left panel: SYS-3 total column liquid water path bias for the JJA 2006 period. Right panel: SYS-4 total column liquid water path bias for the JJA 2006 period

Recent works have identified variations in surface wind driven latent heat flux anomalies as the major factor in driving tropical Atlantic SST variability (Dommenges and Latif, 2000; Frankignoul and Kestenare, 2005; Yu *et al.*, 2006). Thus the root cause of the SST bias does not have to lie with the ocean model HOPE. The atmosphere-ocean system in this region is tightly coupled, with ocean surface temperature anomalies driven by low-level wind biases but in turn affecting the distribution and strength of convection and the associated low-level atmospheric dynamics. The positive feedback of such a two-way coupling between the ocean and atmosphere can amplify the effect of incorrectly represented atmospheric physics.

One such shortcoming in the atmospheric model is apparent from the errors in the short-wave (SW) TOA fluxes (Fig. for system 4 and Fig. for the old SYSTEM 3). A bias exceeding 30 W m^{-2} peak and 10 W m^{-2} over a wide area occurs off the West coast of the continent at 15S in the regions typically covered with stratocumulus cloud and subject to coastal upwelling. Under-estimation of stratocumulus cloud cover and liquid water path is a common global model problem (e.g. Hannay *et al.*, 2009), and the increase in downward SW radiation at the surface would lead to a significant SST warm anomaly. A radiative bias of 30 W m^{-2} distributed over a mixed layer depth of 50m would lead to a bias exceeding 1.5K after a month for example, on the order of the typical model biases.

The errors in the SW budget are confirmed by the model biases in total cloud cover (on the right hand side of the same figures), revealing a significant negative bias in cloud cover in the stratocumulus regions. There is also an underestimate of total column liquid water path in the same regions exceeding 50 g m^{-2} compared to version 6 retrievals from SSM/I (Wentz, 1997) as shown in figure 4.10 .

The surface SW budget is harder to determine from observations over the oceans, however, as the predominant cloud type in this region in JJA is shallow stratocumulus, the TOA biases are likely to reflect those at the surface. The surface downwelling radiation in the region exceeds the (climatology) estimates of da Silva *et al.* (1994) by more than 40 W m^{-2} across the region for example (not shown).

Winds biases are an important factor for determining surface latent and sensible heat fluxes and Huang *et al.* (2004) indicate that wind stress is the major determinant of the SST variability in the Southern Tropical Atlantic (STA) mode. Under-representing local wind speeds leads to inadequate convective

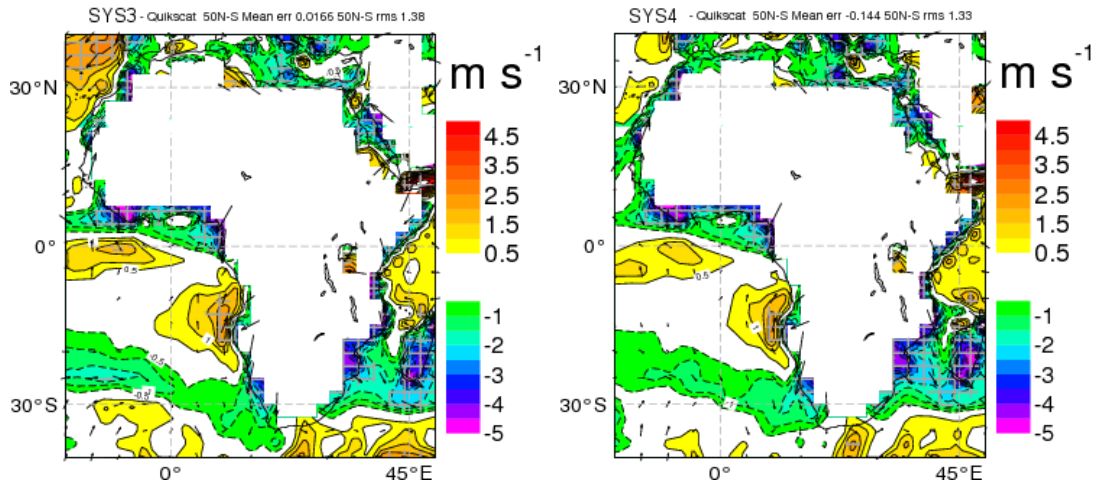


Figure 4.11: Left panel: SYS-3 bias for the 10m wind compared to Quikscat measurements. Right panel: same but for SYS-4. The period refers to JJA 2006.

precipitation in atmosphere-only uncoupled models (Miller *et al.*, 1992). In a coupled model, this is complicated by the fact that surface flux anomalies can not alter the local moist static energy budget integrated across the planetary boundary layer and the ocean surface mixed layer. Thus, although the SST will warm in response to low local wind conditions, while the low wind speeds persist such SST anomalies can not sustain enhanced deep convection. In the coupled system, surface winds also determine the depth of the thermocline and the evolution of the cold equatorial tongue, with low wind speed anomalies on the equator leading to warm anomalies in the Gulf of Guinea (e.g. Verstraete, 1992). Wind stress in the southern Atlantic is also important, and Marin *et al.* (2008) recently contrasted the cold tongue evolutions in 2005 and 2006, showing how the reduced surface wind stress in the southern Atlantic in 2006 led to a late cold tongue development.

A positive wind bias off the West Coast of Africa is seen in Fig. 4.11. This bias extends across the tropical Atlantic south of the equator, although this is smaller than the assumed rms error of the Quikscat instrument retrievals and intra-ensemble spread implying that the systematic biases are not significant there. Moreover this southern Atlantic bias is not apparent when winds are validated using SSM/I retrievals (not shown). In contrast, north of the equator both Satellite retrievals indicate that the model suffers from low wind speeds, with the Quikscat bias vector showing the model has a northerly bias. The monsoon flow is thus weakened in the model, and the pattern of wind biases are consistent with the rainfall biases discussed earlier, with too much convection predicted over the Atlantic leading to the strong convergence zone pattern there. The low wind speeds across the Atlantic north of the equator would lead to reduced surface latent heat fluxes and enhanced SSTs.

In summary, it appears that deficiencies in the model physics that lead to the under-representation of stratocumulus cloud and too low surface winds north of the equator could contribute to the warm SST biases observed during JJA 2006. Assuming very simply that SST biases are locally controlled, then it is possible that the warm bias in the Gulf of Guinea has two distinct origins, with the SW radiative flux errors dominating in the cold tongue region to the south of the equator and wind errors more important north of the equator. Richter and Xie (2008) cite examples of CMIP coupled climate models where this is also the case.

4.2 Surface temperature

The surface temperature is, together with precipitation, the other crucial parameter to drive malaria models. The lack of gridded observations over Africa makes it difficult an assessment of the quality of surface temperature. The comparison is therefore performed here against ERA-I reanalysis. Since the results are similar for both the old SYS-3 and the new SYS-4 only results from this latter model cycle will be shown. Figures 4.12 and ?? show for the 10 year span of validation period the differences in temperatures for the JJA and DJF periods. Remarkly SYS-4 seems to be constantly too cold regardless of the season with the bias augmenting as the time progresses. It has to be noted therefore that ERA-I can be considered as a proxy to observations only up to a certain extend and seasonal invariant temperature bias can be due to inaccuracy in the ERA-I prediction more than to real limitations in the seasonal forecasting system,. This will be analysed in more details in chapter 5.

For the surface temperature a reliability diagrams for SYS-4 is shown for August 2011 for the upper and lower terciles (Figure 4.14). The reliability diagrams measure how closely the forecast probabilities of an event correspond to the actual chance of observing the event. Being based on anomaly this kind of plot is not sensitive to possible biases in ERA interim. The reliability diagram groups the forecasts into bins according to the issued probability (horizontal axis). The frequency with which the event was observed (ERA-I) to occur for this sub-group of forecasts is then plotted against the vertical axis. For perfect reliability the forecast probability and the frequency of occurrence should be equal, and the plotted points should lie on the diagonal (solid line in the figure). Thus, for example, when the forecast states an event will occur with a probability of 25% then for perfect reliability, the event should occur on 25% of occasions on which the statement is made.

In the figure the reliability curves have positive slope, indicating that as the forecast probability of the event occurring increases, so too does the verified chance of observing the event. The forecasts therefore have some reliability. However, the slope is less than the diagonal, indicating less than perfect reliability. For this month when an upper-tercile temperature category has a forecast probability equal to 65% the actual chance of observing the event is closer to 50%.

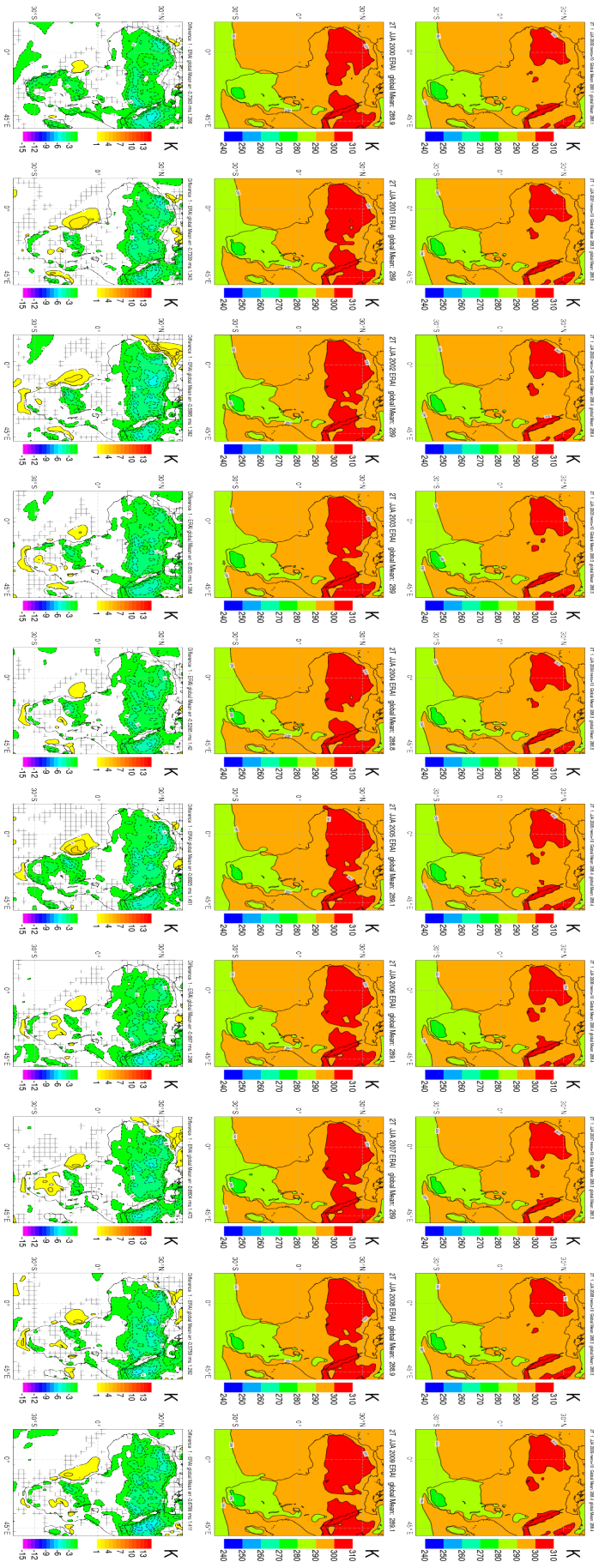


Figure 4.12: System 4 surface temperature bias relative to ERA-I reanalysis for JJA from 2000 to 2009. The hashed area indicate regions where the difference is significant at the 95% level, and negative contours are shown with dashed lines.

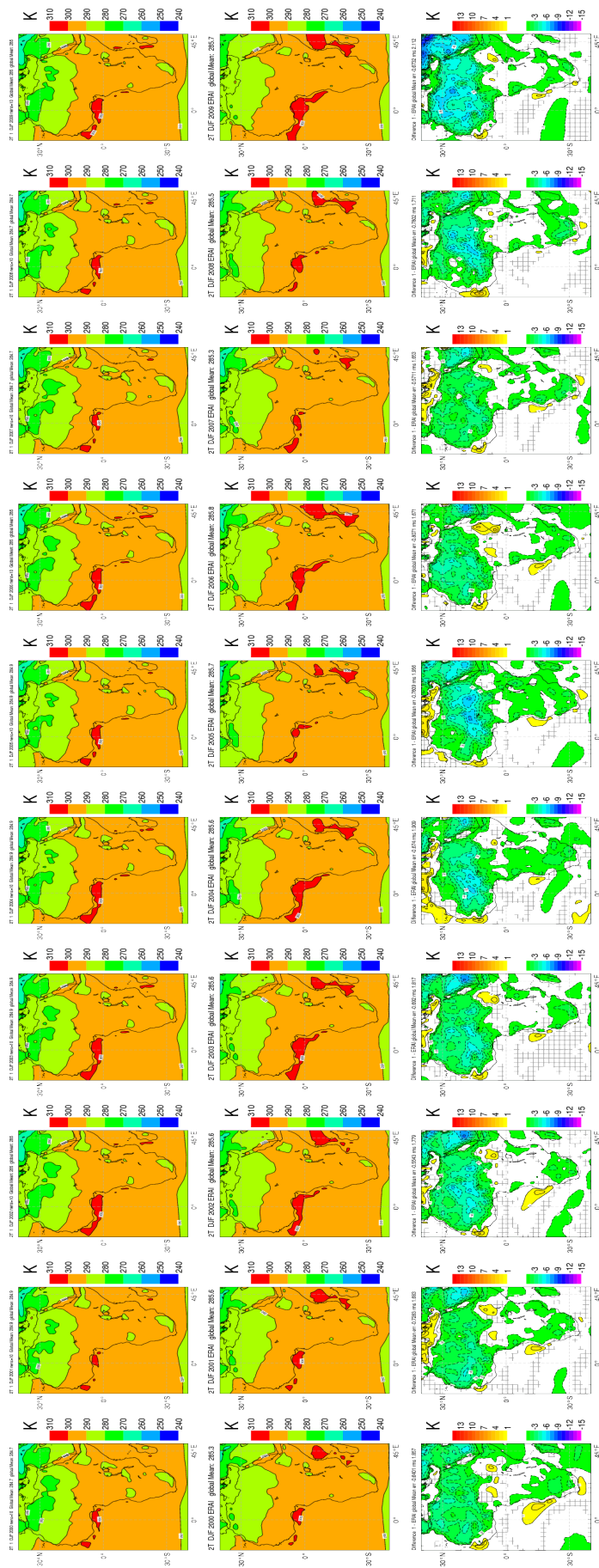
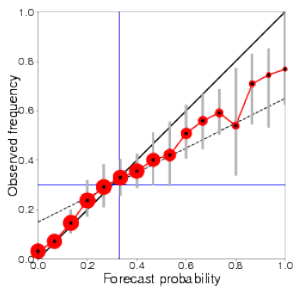


Figure 4.13: Same as figure 4.12 but for the DJF period

Reliability diagram for ECMWF with 15 ensemble members
 Near-surface air temperature anomalies below the lower tercile
 Accumulated over Africa (land points only)
 Hindcast period 1981-2010 with start in December average over months 2 to 4
 Skill scores and 95% conf. intervals (1000 samples)
 Brier skill score: 0.121 (0.026, 0.203)
 Reliability skill score: 0.974 (0.920, 0.993)
 Resolution skill score: 0.147 (0.097, 0.219)



Reliability diagram for ECMWF with 15 ensemble members
 Near-surface air temperature anomalies above the upper tercile
 Accumulated over Africa (land points only)
 Hindcast period 1981-2010 with start in December average over months 2 to 4
 Skill scores and 95% conf. intervals (1000 samples)
 Brier skill score: 0.130 (0.041, 0.206)
 Reliability skill score: 0.982 (0.945, 0.990)
 Resolution skill score: 0.148 (0.088, 0.219)

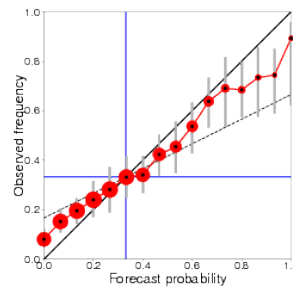


Figure 4.14: Reliability diagrams over Africa (only land points) for SYS-4 initialised the 1st of August 2011 and for months 2 to 4 lead times. Left plot lower tercile. Right plot: upper tercile

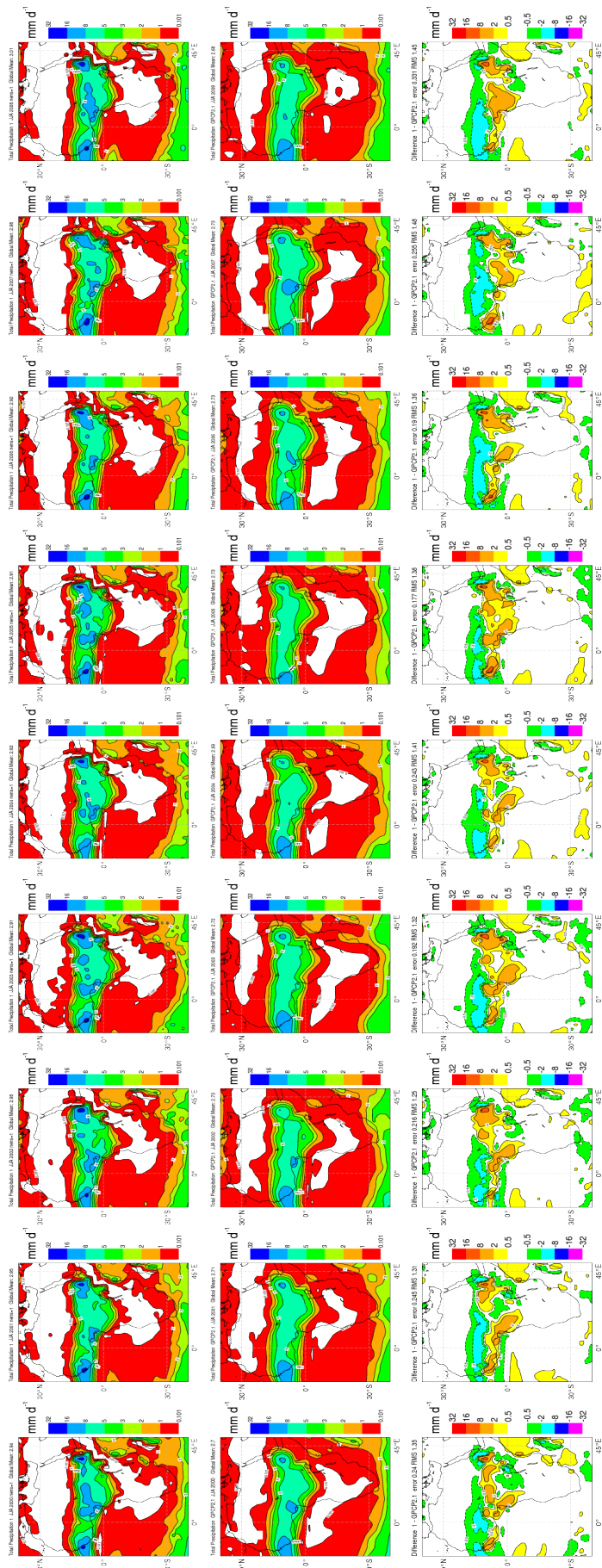


Figure 4.15: ERA-I mean precipitation bias relative to GPCP v2 for JJA from 2000 to 2009. The hashed area indicate regions where the difference is significant at the 95% level, and negative contours are shown with dashed lines.

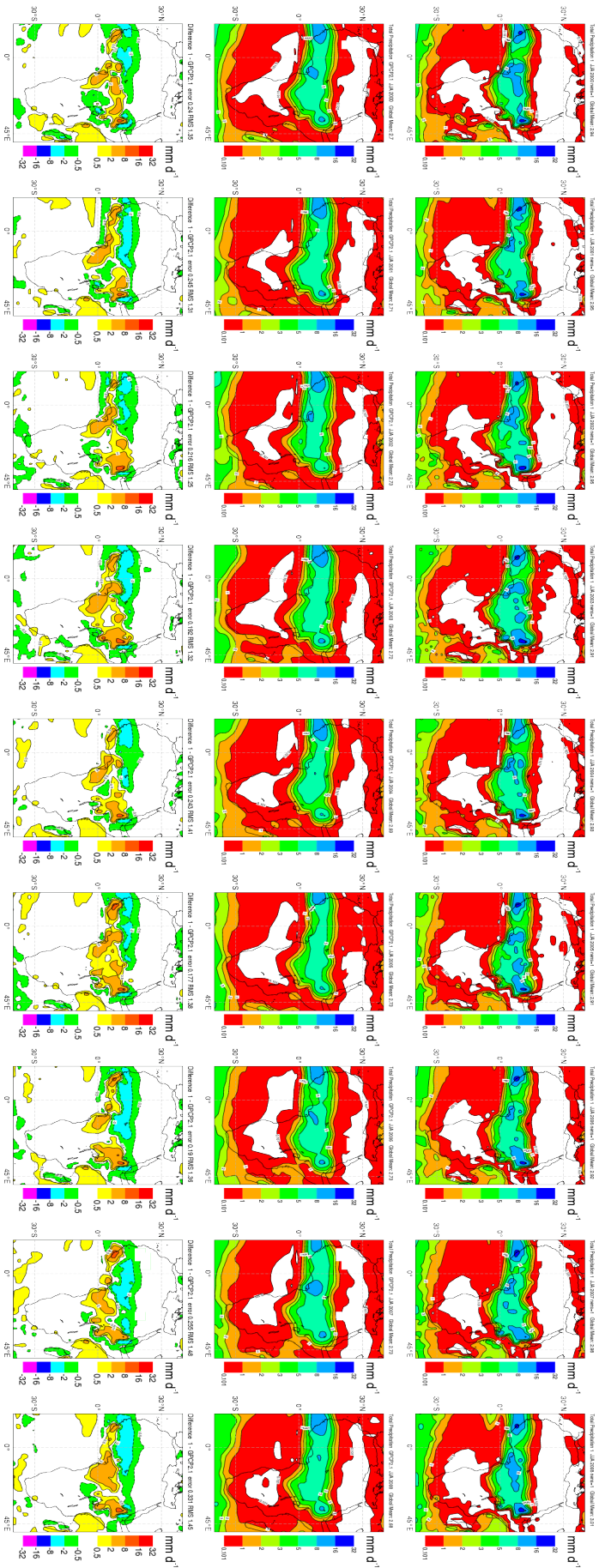


Figure 4.16: ERA-I mean precipitation bias relative to GPCP v2 for JJA from 2000 to 2009. The hashed area indicate regions where the difference is significant at the 95% level, and negative contours are shown with dashed lines.

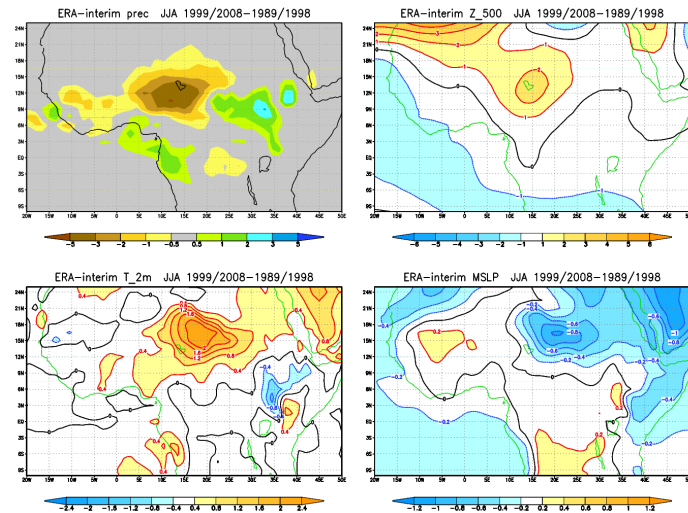


Figure 5.1: Mean ERA-I fields from the last ten year period 1999-2008 compared to the first ten year mean 1989-1998.

5 ERA-I verification

ERA-I precipitation biases for the JJA and DJA seasons and for the whole set of verification years are shown in figures 4.16 and 4.16. The southerly shift in the precipitation for the JJA period is confirmed even if it is less severe than the bias observed in system-3 and 4. This highlights the dependency of the bias on the lead time. Even if Era-I has a nominal lead time of 24 hours it can be considered as an analysis. Therefore much shorter than the lead time of few months considered in the seasonal forecast in the previous chapter. Nevertheless still the bias is evident. This confirms the fact that the bias is generated by the model physics and cannot be corrected by a good model initialisation. The fact that the model is biased can generate systematic model drifts in the reanalysis fields. This is further investigated in figure 5.1 where the first ten years of mean ERA-I fields are compared to the last ten years mean. In the Sahel region the model shows a systematic increase in the 2m temperature and a negative trend in the mean sea level pressure. The pressure minimum and dry biases reduce the precipitation over the Sahel. The dry temperature precipitation bias observed in the 1999-2008 period when compared to the 1989-1999 period can also be due to the interannual climate variability. To highlight how the temperature and precipitation trend is possibly due to the model bias and not real variability in the Africa climatology figures 5.2 and 5.3 show the comparison between ERA-I, the operational ECMWF short range ensemble prediction system (EPS) and the GPCP dataset for the June and July months. The correlation in the precipitation anomaly (calculated using all the years for ERA-I and the ensemble mean for the EPS) shows that the operational forecast has a better correlation with observations than ERA-I. ERA-I correlates as low as 0.01 in July with GPCP while the EPS correlation rises to 0.45.

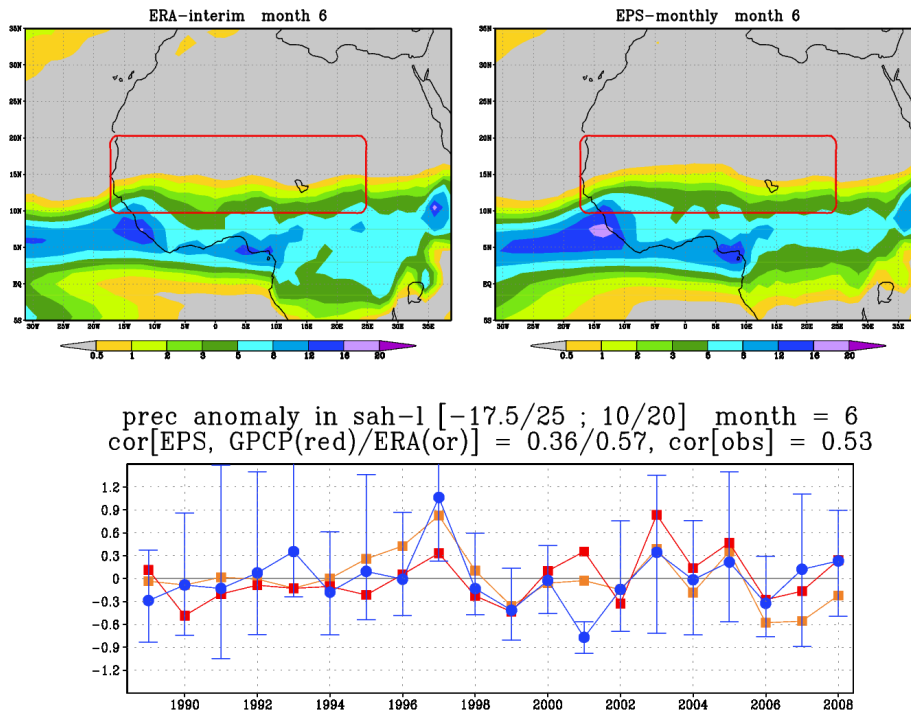


Figure 5.2: Comparison between ERA-I, the operation Ensemble Forecast system (EPS) and GPCP dataset. The upper panel shows the differences between ERA-I and the GPCP climatology for June while the lower panel show the correlation anomaly between the three datasets

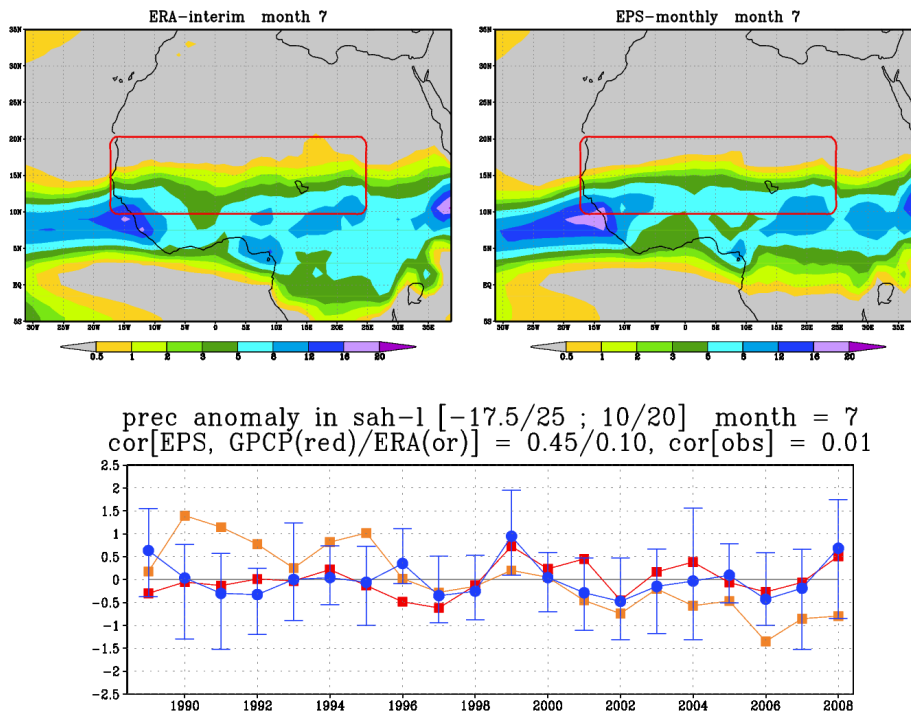


Figure 5.3: Same as figure 5.2 but for July.

6 Conclusion

The ECMWF SYS-4 operational seasonal forecast model has started delivering operational products since November 2011 substituting the old system (SYS-3) which shared the same model cycle of ERA-I. In this report an assessment of the capability of the seasonal forecasting systems and ERA-I to reproduce the climate variability in temperature and precipitation over Africa has been made. The validation has taken in consideration the two main seasons for Africa synoptic regimes; the JJA period relevant for the west Africa monsoon and the DJF in which East Africa is affected by a local monsoon circulation with associated wet season.

Since SYS-4 is the driving atmospheric model chosen to provide the atmospheric fields to drive the malaria models inside the QWECI projects it is important to validate this system in the context of its representation of the African monsoon system. The investigation examined a 10-year set of seasonal hindcasts using 10 ensemble members to examine climatological biases, while additionally documenting some of the specific details of 2006.

Using CMAP, GPCP and TRMM and SSM/I rainfall data, the model was found to reproduce the monsoon progression into the Sahel during July to September, but with a number of differences to the observations. The main one of these was the fact that the model rainfall was displaced to the south, with too much precipitation over the north coast of the Gulf of Guinea during the main monsoon season, and an under-prediction north of 12N. These biases were more evident in the SYS-3 system and have been partially corrected by the new SYS-4 even if they remain still present in both in the long-term model summer climate in the region and specifically in 2006. Concerning the onset and intraseasonal variability, the model did not reproduce the characteristics of the monsoon onset “jump”, and did not show any signs of the period of rainfall depression prior to onset, neither in general, nor in 2006 in particular. The boundary of the smaller rainfall amounts did not undergo any displacement during the onset and remained fixed at approximately 15N throughout most of June, July and August. The skill of predicting the seasonal mean rainfall anomaly in JAS has improved over time in tandem with improvements in the quality of the ocean analysis as Atlantic ocean monitoring increases.

The model forecasts were then compared to a number of other datasets to confirm and attempt to explain the possible origin of some of the rainfall biases, in particular the southerly shift in the monsoon rainfall. Analysis of top of atmosphere IR budgets confirms the rainfall biases although it should be recalled that such datasets contribute to the Satellite rainfall retrieval algorithms and thus do not represent a completely independent dataset.

One possible contributory cause of the southerly rainfall shift was a significant SST bias that develops during the summer months. This bias would tend to enhance deep convection over the Gulf of Guinea northern coasts and suppress rainfall to the north, as seen in the model forecasts. The surface flux budgets revealed that the downwelling SW radiation at the surface was too high in the model off the west coast of Angola, due to a lack of stratocumulus cloud, and it was hypothesised that this could be one contributory factor to the warm SST and associated rainfall biases. It should be emphasised that the operational seasonal forecast SYS3 is using the atmospheric model cycle 31R1 which was operational in the medium

range model during 2006. It is a continuous task of operational centres to attempt to introduce model physics and structure changes to tackle such biases as discussed here, and the medium range and monthly forecast systems since 2006 have incorporated a variety of physics changes which were designed to target known model deficiencies, including the lack of stratocumulus.

The new SYS-4 is in fact capable of improving in most of the previous SYS-3 biases. The new model cycle includes major upgrades to the turbulence mixing scheme, the deep convection scheme and the radiation schemes. These changes were found to significantly improve the simulation of stratocumulus, and alter the balance between convectively parameterised and grid-cell convection. The associated cloud properties changed considerably, which had the result of allowing more SW radiation to reach the surface in deep convecting areas, while reducing it in stratocumulus regimes, although in the latter case this was partially offset by increased downwelling IR from the cloud. The southern Atlantic warm bias in the cold tongue region is improved as a result of the stratocumulus increases. In contrast, the SW increases on and to the north of the equator in deep convective regimes combine with lower winds and latent heat fluxes to make the warm bias significantly worse there. The result is that, while the coupled model is able to increase net precipitation over West Africa, most of the increases are concentrated on the Gulf of Guinea northern coast in JAS, degrading the SYS3 climate which already over-predicted precipitation there during the monsoon season. This highlights the complexity of tackling systematic biases in global coupled models.

Two final points of note to make concern the robustness of the response and the potential to develop seamless forecasting systems. Despite the fact that interannual variability is large in this part of the world, the model biases and the impact of the physics changes dominate and the precipitation bias maps for 2006 were similar for the other ensemble integrations in years between 2000 to 2009, even though the SST state in the Atlantic cold tongue region differed so much between 2005 and 2006. This implies that model developers testing model physics changes, often requiring large volumes of tuning integrations to maximise revised model skill, may presently use a numerically cheap integration framework of a single year, confident in the knowledge that the changes will translate successfully to other years. This will only remain the case while model systematic biases continue to exceed interannual variability.

The final comment concerns the drive towards seamless forecasting, where seamless in this context refers to the use of uniform model physics across a wide range of forecasting timescales (e.g. Vitart *et al.*, 2008) and that has led to milestone **M3.1.a** *Prototype seamless products from monthly to seasonal EPS systems*. and will be re-analysed in the deliverable **D3.1e**. *Report on the seamless calibrated products for disease-related variables integrating the output from medium-range, monthly and seasonal ensemble forecast systems using ECMWF products*.

The ECMWF forecast model has been demonstrated to have a systematic southerly shift in rainfall in coupled mode, and the short range forecasts. However, this bias must have distinct origins in the two systems since integrating the model with imposed SST past two weeks shows a northward migration of the rain-belt to approximately its correct location. Thus methods that assess short-range forecasts to judge climate model integrations such as suggested by Rodwell and Palmer (2007) may not be valid if a short-range uncoupled model is used to assess a coupled system.

The changes that were made in between the 2006 model cycle 31R1 and the more recent cycle 36R4 were selected and implemented after an exhaustive development and testing regime that showed a net gain in medium-range forecast skill in the uncoupled system. These changes, when implemented in a revised seasonal forecasting system, can cause deterioration in some aspects of the modelled Africa climate for example. This highlights the complexity of developing physical parametrisations that can perform

well in both coupled and uncoupled models across a wide range of timescales in the so-called seamless forecast approach, especially if the performance metric by which the models are judged also changes with timescale.

As there is an increasing determination to apply seasonal forecasting systems fruitfully to the impacts sectors of health, water, energy and agriculture (e.g. Jones *et al.*, 2000; Ingram *et al.*, 2002; Thomson *et al.*, 2006; Millner and Washington, 2010; Lamb *et al.*, 2010). Despite the improvements seen in SYS-4 compared to SYS-3, the predicted fields such as temperature and precipitation that are required to drive sectoral models are still biased, and thus require correction. The development of new bias correction techniques for precipitation has already started in the QWECI projects and report **D3.1e**. will address the particularly demanding problem of precipitation bias correction for Africa.

Bibliography

- Adler RF, Huffman GJ, Chang A, Ferraro R, Xie PP, Janowiak J, Rudolf B, Schneider U, Curtis S, Bolvin Dea. 2003. The version-2 global precipitation climatology project (GPCP) monthly precipitation analysis (1979–present). *J. Hydrometeor.* **4**: 1147–1167.
- Albignat JP, Reed RJ. 1980. The origin and structure of easterly waves in the lower troposphere in North Africa. *Mon. Wea. Rev.* **108**: 1827–1839.
- Blanke B, Delecluse P. 1993. Variability of the tropical Atlantic ocean simulated by a general circulation model with two different mixed-layer physics. *J. Physical Ocean.* **23**: 1363–1388.
- Burpee R. 1972. The origin and structure of easterly waves in the lower troposphere of North Africa. *J. Atmos. Sci.* **29**: 77–90.
- Chevallier F, Kelly G. 2002. Model clouds as seen from space: Comparison with geostationary imagery in the 11-micron window channel. *Mon. Wea. Rev.* **130**: 712–722.
- da Silva A, Young CC, Levitus S. 1994. Atlas of surface marine data 1994. Vol 1: Algorithms and procedures. Technical report, US Department of Commerce, Washinton DC. pp83.
- Dee DP, Uppala SM, Simmons AJ, Berrisford P, Poli P, Kobayashi S, Andrae U, Balmaseda MA, Balsamo G, Bauer P, coauthors. 2011. The era-interim reanalysis: configuration and performance of the data assimilation system. *Q. J. R. Meteorol. Soc.* **137**(656): 553–597.
- Dommenget D, Latif M. 2000. Interannual to decadal variability in the tropical Atlantic. *J. Climate* **13**: 777–792.
- Douville H, Chauvin F. 2000. Relevance of soil moisture for seasonal climate predictions: a preliminary study. *Climate Dynamics* **16**: 719–736.
- Frankignoul C, Kestenare E. 2005. Air–sea interactions in the tropical Atlantic: A view based on lagged rotated maximum covariance analysis. *J. Climate* **18**: 3874–3890.
- Giannini A, Saravanan R, Chang P. 2003. Oceanic forcing of Sahel rainfall on interannual to interdecadal time scales. *Science* **302**: 1027–1030.
- Hannay C, Williamson DL, Hack JJ, Kiehl JT, Olson J, Klein SA, Bretherton C, K
"ohler M. 2009. Evaluation of forecasted southeast Pacific stratocumulus in the NCAR, GFDL and ECMWF models. *J. Climate* **22**: 2871–2889.
- Held IM, Delworth TL, Lu J, Findell KL, Knutson TR. 2005. Simulation of Sahel drought in the 20th and 21st centuries. *Proc. Nat. Acad. Sci.* **102**: 17 891–17 896.
- Hoffman RN, Leidner SM. 2005. An introduction to the near-real-time QuikSCAT data. *Wea. and Forecasting* **20**: 476–493.

- Houze Jr R, Betts A. 1981. Convection in gate. *Reviews of Geophysics* **19**(4): 541–576.
- Huang B, Schopf PS, Shukla J. 2004. Intrinsic ocean–atmosphere variability of the tropical Atlantic Ocean. *J. Climate* **17**: 2058–2077.
- Huffman GJ, Adler R, Rudolph B, Schneider U, Keehn P. 1995. Global precipitation estimates based on a technique for combining satellite-based estimates, rain gauge analysis, and NWP model precipitation information. *J. Climate* **8**: 1284–1295.
- Ingram KT, Roncoli MC, Kirshen PH. 2002. Opportunities and constraints for farmers of west africa to use seasonal precipitation forecasts with burkina faso as a case study. *Agricultural Systems* **74**(3): 331–349.
- Janicot S, Thorncroft CD, Ali A, Asencio N, Berry G, Bock O, Bourles B, Caniaux G, Chauvin F, Deme A, Kergoat L, Lafore JP, Lavaysse C, Lebel T, Marticorena B, Mounier F, Nedelec P, Redelsperger JL, Ravegnani F, Reeves CE, Roca R, de Rosnay P, Schlager H, Sultan B, Tomasini M, Ulanovsky A, Acmad Forecasters Team. 2008. Large-scale overview of the summer monsoon over West Africa during the AMMA field experiment in 2006. *Ann. Geophysicae* **26**: 2569–2595.
- Jones JW, Hansen JW, Royce FS, Messina CD. 2000. Potential benefits of climate forecasting to agriculture. *Agriculture, ecosystems & environment* **82**(1-3): 169–184, doi:DOI: 10.1016/S0167-8809(00)00225-5.
- Laing A, Fritsch J. 1993. Mesoscale convective complexes in africa. *Monthly Weather Review;(United States)* **121**(8).
- Lamb P, Timmer RP, Lele MI. 2010. Professional development for climate prediction and projection. *Climate Res.* **47**: 57–75, doi: 10.3354/cr00949.
- Marin F, Caniaux G, Bourlès B, Giordani H, Gouriou Y, Key E. 2008. Why were sea surface temperatures so different in the eastern equatorial Atlantic in June 2005 and 2006? *J. Physical Ocean.* **39**: 1416–1431.
- Miller MJ, Beljaars ACM, Palmer TN. 1992. The sensitivity of the ECMWF model to the parameterization of evaporation from the tropical oceans. *J. Climate* **5**: 418–434.
- Millner A, Washington R. 2010. What determines perceived value of seasonal climate forecasts? a theoretical analysis. *Global Environmental Change* .
- Mitchell TD, Jones PD. 2005. An improved method of constructing a database of monthly climate observations and associated high-resolution grids. *Int. J. Climatol.* **25**: 693–712.
- Mitchell TP, Wallace JM. 1992. The annual cycle in equatorial convection and sea surface temperature. *J. Climate* **5**: 1140–1156.
- Morcrette J. 1989. Comparison of satellite-derived and model-generated diurnal cycles of cloudiness and brightness temperatures. *Advances in Space Research* **9**: 175–179.
- Norquist D, Recker E, Reed R. 1977. The energetics of african wave disturbances as observed during phase iii of gate(baroclinic and barotropic energy conversions). *Monthly Weather Review* **105**: 334–342.
- Okumura Y, Xie SP. 2004. Interaction of the Atlantic equatorial cold tongue and the African monsoon. *J. Climate* **17**: 3589–3602.

- Palmer TN. 1986. Influence of the Atlantic, Pacific and Indian Oceans on Sahel rainfall. *Nature* **322**: 251–253.
- Parker DJ. 2002. The response of CAPE and CIN to tropospheric thermal variations. *Q. J. R. Meteorol. Soc.* **128**: 119–130.
- Parker DJ, Burton RR, Diongue A, Ellis RJ, Felton M, Taylor CM, Thorncroft CD, Bessemoulin P, Tompkins AM. 2005. The diurnal cycle of the West African Monsoon circulation. *Q. J. R. Meteorol. Soc.* **131**: 2839–2860.
- Rennick M. 1981. Some sensitivity experiments with an african wave model. *Journal of Atmospheric Sciences* **38**: 106–113.
- Reynolds RW, Rayner NA, Smith TM, Stokes DC, Wang W. 2002. An improved in situ and satellite SST analysis. *J. Climate* **15**: 1609–1625.
- Richter I, Xie SP. 2008. On the origin of equatorial Atlantic biases in coupled general circulation models. *Climate Dynamics* **31**: 587–598.
- Rodwell MJ, Palmer TN. 2007. Using numerical weather prediction to assess climate models. *Q. J. R. Meteorol. Soc.* **133**.
- Rossow WB, Schiffer RA. 1991. ISCCP cloud data products. *Bull. Amer. Meteor. Soc.* **72**: 2–20.
- Rossow WB, Walker AW, Garder LC. 1993. Comparison of ISCCP and other cloud amounts. *J. Climate* **6**: 2394–2418.
- Thomson MC, Doblas-Reyes FJ, Mason SJ, Hagedorn R, Connor SJ, Phindela T, Morse AP, Palmer TN. 2006. Malaria early warnings based on seasonal climate forecasts from multi-model ensembles. *Nature* **439**: 576–579.
- Thorncroft CD, Parker DJ, Burton RR, Diop M, Hayers JH, Barjat H, Dumelow R, Kindred DR, Price NM, Taylor CM, Tompkins AM. 2003. The JET2000 project: Aircraft observations of the African easterly jet and African easterly waves. *Bull. Amer. Meteor. Soc.* **84**: 337–351.
- Tompkins AM, Cardinali C, Morcrette JJ, Rodwell M. 2005. Influence of aerosol climatology on forecasts of the African easterly jet. *Geophys. Res. Lett.* **32**: L10 801, doi:10.1029/2004GL022 189.
- Verstraete JM. 1992. The seasonal upwellings in the Gulf of Guinea. *Progress in Oceanography* **29**: 1–60.
- Vialard J, Vitart F, Balmaseda MA, Stockdale TN, Anderson DLT. 2005. An ensemble generation method for seasonal forecasting with an ocean–atmosphere coupled model. *Mon. Wea. Rev.* **133**: 441–453.
- Vitart F, Buizza R, Alonso Balmaseda M, Balsamo G, Bidlot JR, Bonet A, Fuentes M, Hofstadler A, Molteni F, Palmer TN. 2008. The new VarEPS-monthly forecasting system: A first step towards seamless prediction. *Q. J. R. Meteorol. Soc.* **134**(636): 1789–1799.
- Wentz FJ. 1997. A well-calibrated ocean algorithm for SSM/I. *J. Geophys. Res.* **102**: 8703–8718.
- Wielicki BA, Barkstrom BR, Harrison EF, Lee RB, Smith GL, Cooper JE. 1996. Clouds and the earth's radiant energy system (CERES): An earth observing system experiment. *Bull. Amer. Meteor. Soc.* **77**: 853–868.

- Wielicki BA, Cess RD, King MD, Randall AD, Harrison EF. 1995. Mission to planet Earth: Role of clouds and radiation in climate. *Bull. Amer. Meteor. Soc.* **76**: 2125–2153.
- Wolff JO, Maier-Reimer E, Legutke S. 1997. *The Hamburg Ocean Primitive Equation Model*. DKRZ.
- Xie P, Arkin PA. 1997. Global precipitation: A 17-year monthly analysis based on gauge observations, satellite estimates, and numerical model outputs. *Bull. Amer. Meteor. Soc.* **78**: 2539–2558.
- Yu L, Jin X, Weller RA. 2006. Role of net surface heat flux in seasonal variations of sea surface temperature in the tropical Atlantic ocean. *J. Climate* **19**: 6153–6169.